JOURNAL OF MAGNETIC RESONANCE, Series A **121,** 33–41 (1996)
ARTICLE NO. 0132

Excitation-Sculptured Indirect-Detection Experiment (EXSIDE) for Long-Range CH Coupling-Constant Measurement

V. V. KRISHNAMURTHY

Gilead Sciences, 353 Lakeside Drive, Foster City, California 94404

Received January 22, 1996

A new pulse sequence (*ex*citation-*s*culptured *i*ndirect-*d*etection *e*xperiment, EXSIDE) for measuring long-range heteronuclear coupling constants has been proposed. The experiment is a band-selective variant of the gradient–HSQC experiment. The initial polarization transfer from ^{1}H to ^{13}C and the refocusing of the antiphase ^{1}H magnetization after the back-transfer from ^{13}C to ^{1}H is unmodulated by any passive homonuclear couplings. This is achieved by a variation of the double pulse-field-gradient spin-echo technique. The sequence provides pure absorptive lineshapes, and long-range heteronuclear coupling constants are *J*-scaled and measured along the F_1 (carbon) dimension. Unlike methods where the heteronuclear couplings are extracted along the F_2 (proton) dimension with overlapping homonuclear couplings, in the EXSIDE spectrum the active coupling constant is measured with no interference from any passive couplings. As long as one can group subsets of resonances that are not coupled to each other, the method can be used with multifrequency selection. The applicability of the experiment to measure $^{n}J_{CH}$ is demonstrated using strychnine. The unique chemical-shift region of anomeric protons in oligosaccharides and the H1′ protons in oligonucleotides makes this method easily applicable for measuring long-range CH coupling constants across the glycosidic bond.

INTRODUCTION

Two-dimensional proton–carbon (one-bond and long-range) chemical-shift correlation spectra are important tools in structural determination (*1–3*). Proton-detected heteronuclear experiments (such as HMQC and HMBC) offer substantial sensitivity enhancement over carbon-detected experiments (*4–9*). The resolution along the carbon dimension in proton-detected experiments is generally low and controlled by the number of t_1 increments. The total experiment time must be doubled to increase this resolution by a factor of two. In spite of this, these experiments have become the methods of choice, because the large chemical-shift dispersion along the carbon dimension allows one to resolve the signals even if the digital resolution is poor.

In addition to carbon and proton chemical shifts and their ''connectivity'' in direct and long-range correlation spectra, homonuclear and heteronuclear coupling constants offer a wealth of structural information (*10*). They can provide information on dihedral angles via a Karplus equation (*11*). New proton-detected methods have been presented in recent years to determine long-range heteronuclear coupling constants. The J_{CH} can be obtained from E.COSY-like signal splitting with $^{1}J_{XH}$ in F_1 and $^{n}J_{XH}$ in F_2. Signals of this kind appear in X-filtered NOESY (*12, 13*) or X-filtered TOCSY (*14–16*) experiments and can be combined with editing and selection techniques (*17–19*). These experiments, however, are applicable only to protonated carbons. Various other 1D, 2D, and 3D techniques based on HMBC and HSQC experiment have also been proposed (*20–27*). The focus in these cases is to extract the heteronuclear coupling constants in the presence of homonuclear couplings. This is typically achieved by lineshape analysis (in the proton-detection dimension) or signal-intensity analysis (analytical, 2D, or 3D methods) or by the use of selective excitation (in the proton and/or carbon dimensions). A recent review (*28*) surveys the various methods for determining scalar coupling constants (including heteronuclear coupling constants) and their analysis and application for the elucidation of structures.

In principle, heteronuclear long-range coupling constants can be measured directly from the cross peaks in HMBC spectra. If the desired heteronuclear coupling is to be extracted from the cross peaks along the proton dimension using HMBC or HSQC sequences, the experiment must be run without ^{13}C decoupling and preferably without the long refocusing delay. Long-range heteronuclear coupling constants are approximately of the same magnitude as homonuclear coupling constants. Therefore, the rather small heteronuclear antiphase coupling constants are difficult to measure because of overlapping (and reciprocal cancellation) of the numerous multiplet lines. Moreover, the nonrefocused multiplet of an HMBC cross peak is not purely absorptive in phase in F_2 because of the modulation through homonuclear couplings and through the development of the proton chemical-shift evolution during the polarization-transfer delay. While the proton chemical shifts can be refocused by using the refocused version, the homonuclear coupling evolution cannot be refocused.

It is even more difficult to measure the desired coupling

1064-1858/96 $18.00

constant along the carbon dimension, as this would require a selective proton π pulse during the evolution period to refocus all but the ''active'' proton. This problem was recently circumvented in the gs-*J*-HMBC sequence (*27*). In this modification of gradient-selected HMBC (*29, 30*), the coupling constant is measured along an additional evolution (or pseudo evolution) dimension. Use of gradients, as in the gs-*J*-HMBC experiment, to select the coherence pathway also substantially improves the suppression of the magnetization of protons not coupled to ^{13}C, which often produces intense t_1 noise and interferes with the coupling constant measurement. Modifications of HSQC experiments to generate pure absorption-mode spectra in both F_1 and F_2 dimensions and measure the heteronuclear couplings along the proton dimension have also been proposed (*24, 26*). The interference of in-phase homonuclear couplings with the antiphase heteronuclear couplings still exists as long as one attempts to measure the heteronuclear couplings along the proton dimension.

We now wish to report an *ex*citation-*s*culptured *i*ndirect-*d*etection *e*xperiment (EXSIDE) that provides cross peaks which are *J*-scaled in the carbon dimension. This experiment is a semiselective version of the gradient-selected HSQC sequence (*31, 32*). Proton band selection is based on the excitation-sculpting technique (*33*) reported by Shaka *et al.* The experiment is run with ^{13}C decoupling during acquisition and generates a spectrum that is purely absorptive in both F_1 and F_2 dimensions. All heteronuclear couplings are refocused during the ^{13}C evolution. Cross peaks appear as doublets along the F_1 dimension centered at the ^{13}C chemical shift. The frequency separation of the doublet components is the active CH long-range coupling constant scaled up by a factor predefined by the user.

PULSE SEQUENCE

The EXSIDE pulse sequence used for the measurement of long-range range CH coupling constants is shown in Fig. 1A. The EXSIDE experiment, in principle, involves the following steps: (i) selective INEPT (*34*) from protons to carbon; (ii) carbon evolution; (iii) gradient encoding; (iv) polarization transfer back to protons; (v) gradient decoding; (vi) selective refocusing of the antiphase proton magnetization; and (vii) proton observation with ^{13}C decoupling. The coherence-pathway selection is done using magnetic field gradients. Data from N- and P-type coherence pathways were collected separately (by inverting the sign of the decoding gradient pulse) and combined during processing to generate pure absorption lineshapes (*31, 32*). During the selective INEPT (step i), the polarization-transfer efficiency is *J*-modulated in amplitude during the period τ. By setting τ as a function of t_1 ($\tau = N \times t_1$), the observed magnetization is frequency modulated by the ^{13}C chemical shift and amplitude modulated by $N \times J$.

The selective INEPT (step i) and selective refocusing (step vi) are achieved using a modification of the double PFG spin-echo (DPFGSE) technique (*33*). In the absence of the carbon π pulses during the DPFGSE train (as shown in Fig. 1B), the proton magnetization returns to its starting position at the end of the DPFGSE train, the excitation profile depending only on the inversion profile of the band-selective proton π pulses. The phase of the magnetization is unaffected while the amplitude is scaled by the inversion profile of these band-selective π pulses and by any relaxation loss. Multiple resonances can be simultaneously inverted by appropriate choice of ''multiple-frequency''-shifted laminar pulses (*35*). An increase in the length of the echo delays (Δ_1 and/or Δ_2) affects only the amplitude of the magnetization (due to increased loss through relaxation), as long as only resonances that are not coupled to each other are selected (which can be typically achieved by examining a COSY spectrum).

When carbon π pulses are introduced simultaneously with the band-selective proton π pulses, as in the EXSIDE sequence, Fig. 1A, the proton–carbon coupling continues to evolve during Δ. At the end of Δ, the proton magnetization can be transferred to carbon by a pair of $\pi/2$ pulses. Since only proton resonances that are not coupled to each other are intentionally chosen by the band-selective pulse, the polarization-transfer efficiency is modulated only by the term $\sin(\pi J\Delta)$ with maximum transfer when $\Delta = 1/2J$ and is unmodulated by any passive homonuclear coupling. On the same score, the refocusing of the antiphase proton magnetization after the back-transfer to protons is unmodulated by any passive homonuclear coupling, thus retaining the pure in-phase characteristic of the detected homonuclear multiplet.

The EXSIDE sequence incorporates, in effect, two evolution periods (τ and t_1). During the period τ, an amplitude modulation is introduced into the polarization-transfer efficiency that is a function of the active heteronuclear coupling constant. By setting $\tau = N \times t_1$, where N is the *J*-scaling factor, this amplitude modulation is observed in the F_1 dimension along with the ^{13}C chemical shift. The cross peaks appear in the F_1 dimension, at their ^{13}C chemical shifts, as doublets with a frequency separation of $N \times J$. This approach for combining the *J*-modulation dimension and the ^{13}C chemical-shift dimension parallels the accordion experiment reported earlier (*36*).

The EXSIDE sequence (Fig. 1A) also incorporates a gradient pulse between the proton and carbon $\pi/2$ pulses during the polarization-transfer step, improving the suppression of proton magnetization not coupled to ^{13}C (*37*). A TANGO (*38*) train for exciting protons that are directly attached to ^{13}C followed by a gradient pulse (not shown in Fig. 1A) typically precedes the sequence. This eliminates any unwanted one-bond correlations from the spectrum. In EXSIDE spectra with single-resonance selection, one-bond cor-

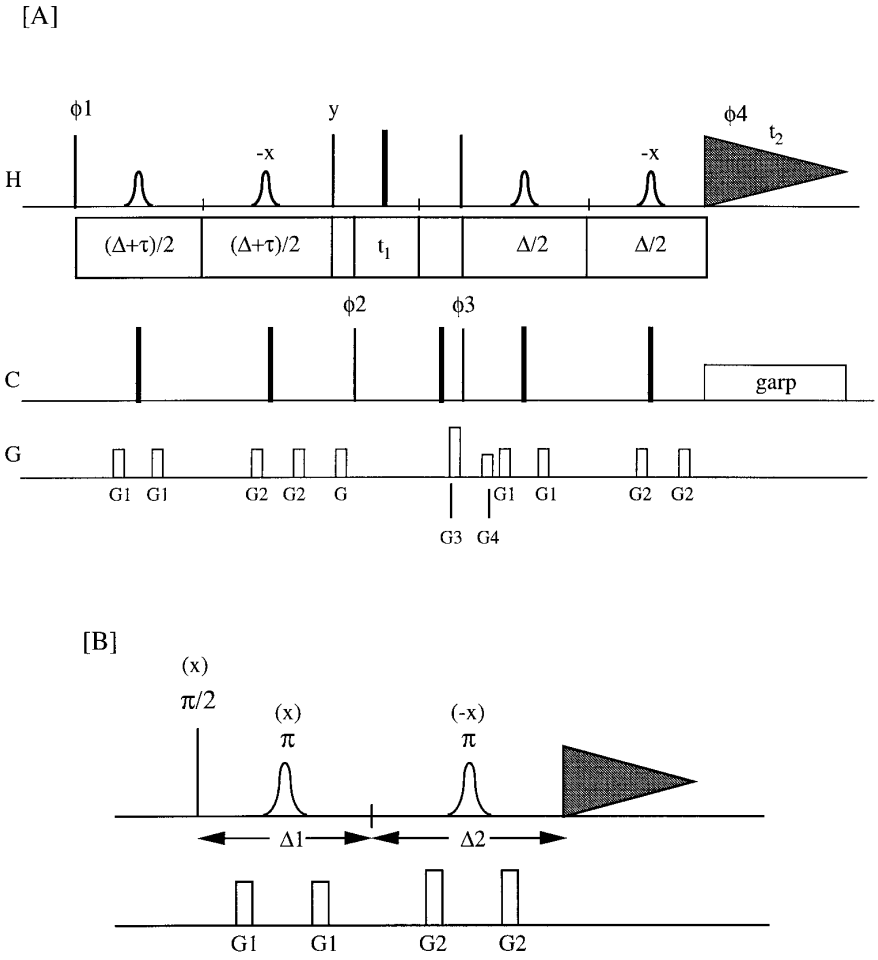

FIG. 1. [A] The EXSIDE pulse sequence. Unless otherwise indicated, the thin and thick vertical lines represent 90° and 180° pulses, respectively. The band-selective proton pulses during Δ are π pulses. The basic phase cycling is $\phi_1 = x, x, x, x, -x, -x, -x, -x$; $\phi_2 = x, x, -x, -x$; $\phi_3 = x, -x$; and $\phi_4 = x, -x, -x, x, -x, x, x, -x$. Phases not shown are along the x axis. Pure N- and P-type data were collected (by inverting the sign of the G_4 gradient), stored separately, and combined during processing to generate pure absorptive lineshapes. [B] Basic double PFG spin echo (DPFGSE).

relations can be easily avoided by judicious choice of an excitation bandwidth narrower than $^1J_{CH}$. However, when semiselective excitations or multiple-frequency excitations are used, it is not always possible to avoid excitation of $^1J_{CH}$ satellites. Such one-bond correlations will appear as doublets with substantially large frequency separation ($=N \times {}^1J_{CH}$) and, thus, can lead to misinterpretation. Use of a TANGO–gradient pair eliminates this ambiguity.

RESULTS AND DISCUSSION

The key to the success of the EXSIDE sequence relies on the ability to selectively defocus only the heteronuclear coupling without any homonuclear J modulation prior to INEPT transfer. In addition, generation of pure absorption-mode proton magnetization also relies on the ability to selectively refocus only the heteronuclear coupling without any homonuclear J modulation during the refocusing period after the back-transfer to proton. Both these requirements are accomplished by the DPFGSE pulse train. The ability of the DPFGSE pulse train to excite multiplet resonances with clean phase properties (independent of the length of the DPFGSE train) is demonstrated, using a sample of strychnine, in Fig. 2. All selective-inversion pulses are frequency (single or multiple frequencies, as the case may be) shifted Q3 pulses (*39*), generated using the Pandora's Box (*40*) pulse-shaping program available in Varian NMR software. As can be seen, independent of the length of the π pulse or the number of resonances inverted, the DPFGSE pulse train generates pure-phase lineshapes. Selective excitation using the DPFGSE train require no phase cycling. All selective-excitation spectra in Fig. 2 were recorded with one scan each. As pointed out earlier, when more than one resonance is inverted by a multiple-frequency-shifted shaped pulse,

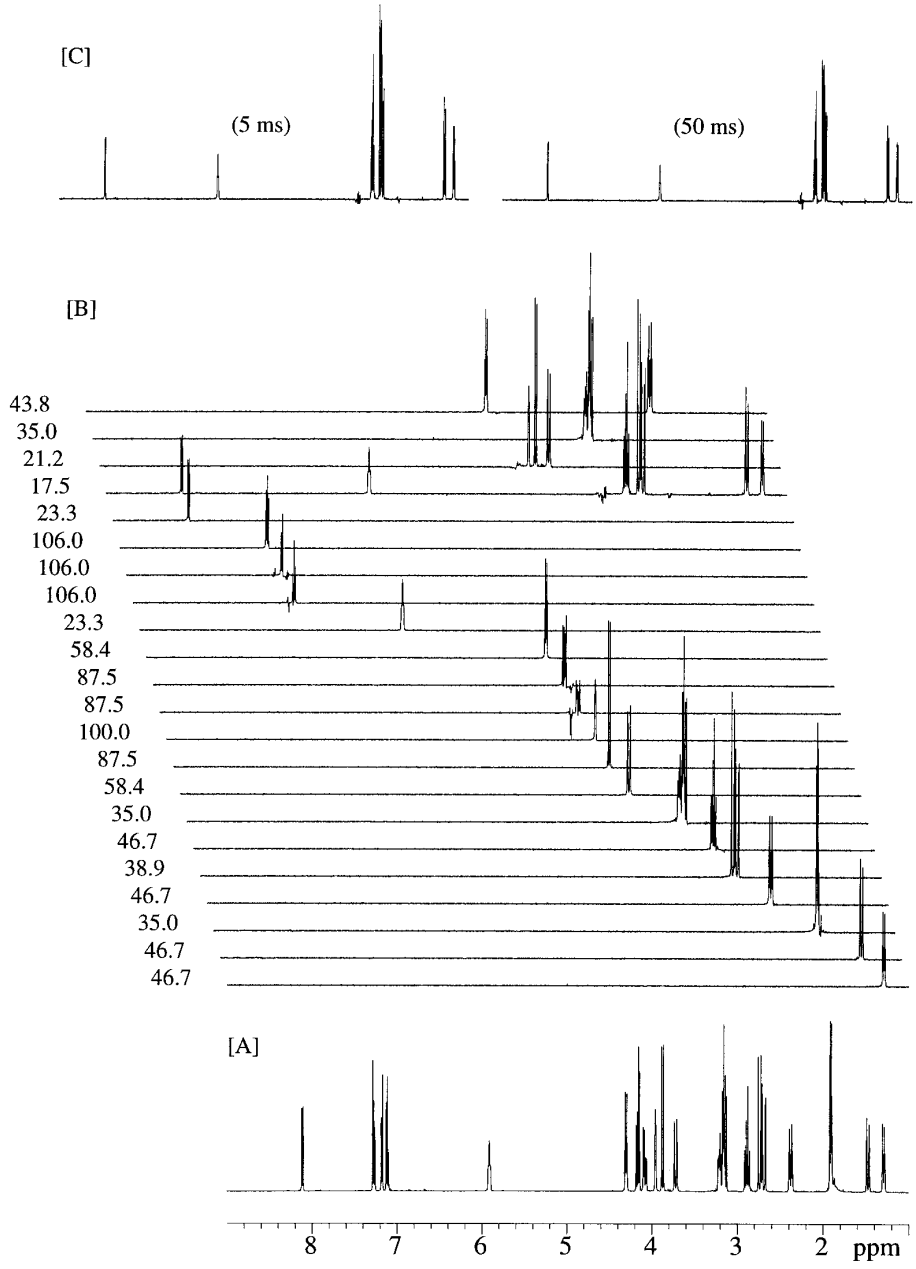

FIG. 2. One-dimensional spectra of strychnine in $CDCl_3$: [A] High-resolution reference spectrum; [B] single- or multiple-frequency-selected 1D spectra using the DPFGSE technique. The lengths of the band-selective π pulses are given in ms with each spectrum. These are Q3 pulses with phase modulation (*35*) to invert the selected resonance(s). The length of the echo delays, Δ_1 and Δ_2, is 2 ms (inclusive of the gradient time) each. [C] Multiple-frequency-selected 1D spectra with 5 and 50 ms echo delays ($\Delta_1 = \Delta_2 = 5$ or 50 ms). All spectra in B and C are run with one scan each and plotted with the same vertical scaling factor.

only those resonances that are not coupled to each other are chosen. This was achieved by an examination of the COSY spectrum (not shown). In the case of strychnine, all aliphatic resonances (except two closely spaced AB methylene protons) can be grouped into four sets. Thus, the pure-phase characteristic of the resonances is retained, independent of the length of the echo delays in the DPFGSE train. However, resonances with short T_2^* are expected to have substantial amplitude loss with longer echo delays.

The EXSIDE sequence was tested using a sample of phenylalanine (^{13}C enriched at the β carbon). In this sample, frequency separation between the H_α and the ^{13}C satellite of the most downfield H_β resonance is 190 Hz. A 35 ms Q3 inversion pulse (measured inversion bandwidth is approxi-

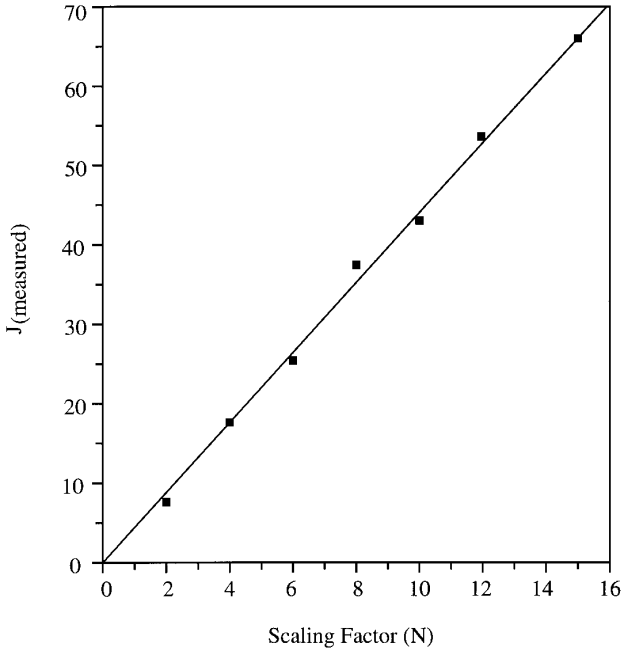

FIG. 3. Plot of scaling factor (N) vs the measured frequency separation between the doublet components (J_{measured}) of the $H_\alpha-C_\beta$ cross peak in the EXSIDE spectra of phenylalanine. The slope of the plot (4.42 Hz) compares well with the coupling constant measured (4.4 Hz) from the 1D proton spectrum.

mately 100 Hz) is used. A series of EXSIDE spectra were recorded using varying values of the *J*-scaling factor, and the frequency separation between the doublet components of the $H_\alpha-C_\beta$ cross peak was measured. Figure 3 shows excellent correlation between the coupling constant obtained (the slope of the plot is 4.42 Hz) from the EXSIDE spectrum and the actual coupling constant (4.4 Hz measured directly from a high-resolution proton spectrum).

In Fig. 4, results from EXSIDE spectra of strychnine are compared with a gradient-selected magnitude-mode HMBC spectrum (*29, 30*). The EXSIDE spectrum shown is, in fact, a superposition of four EXSIDE spectra collected using four different band selections. Each of these four EXSIDE spectra and the HMBC spectrum were collected over the same total acquisition time. All cross peaks in the HMBC spectrum were observed in the EXSIDE spectrum with relatively similar intensity. Less sensitivity is expected in the EXSIDE spectrum compared to the HMBC spectrum due to increased length of the sequence and hence increased loss due to relaxation. However, the EXSIDE spectra can be processed in purely absorptive mode and hence have better lineshapes, while the HMBC spectra are typically processed in the magnitude mode with severe resolution enhancement weighting. In the present case, the EXSIDE spectra were processed with unshifted Gaussian functions (sensitivity-enhancement weighting) while the HMBC spectrum was processed with unshifted sine-squared functions (resolution-enhancement weighting), in both F_1 and F_2 dimensions. This more than compensates for the loss of signal due to relaxation in the EXSIDE spectrum compared to the HMBC spectrum. However, the EXSIDE spectrum cannot be run with all the proton resonances. The proton spectrum must be divided into multiple subsets of resonances that do not have homonuclear coupling between them. This is an intrinsic limitation of the EXSIDE sequence. Expansions of selected cross peaks from the EXSIDE spectra are given in Fig. 5. Coupling constants that are larger than $1/\tau_{(\max)}$ [i.e., $1/(N \times t_{1(\max)})$] can be measured.

In oligosaccharides, the long-range carbon–proton coupling constants through the glycosidic bonds are valuable parameters in conformational analysis. In oligonucleotides, the long-range carbon–proton coupling constants between H1′ and the base carbons (C2/C6 in pyrimidines and C8/C4 in purines) can be used to analyze the glycosidic angle χ. In both these classes of compounds, the protons of interest (anomeric protons in the former case and H1′ in the later case) have a unique chemical-shift region in the proton spectrum. They can be conveniently band-selected and the long-range coupling constants can be measured using the EXSIDE sequence. In Fig. 6, the EXSIDE spectrum of one example of each of these two classes of compounds is given. The sensitivity of the EXSIDE spectrum is dependent on the relaxation times, and hence its applicability is expected to be limited to small molecules.

The EXSIDE sequence can be modified by introducing band-selective carbon π pulses during the polarization transfer and refocusing delays or band-selective carbon $\pi/2$ pulses during the polarization-transfer step(s). This will enable one to narrow the carbon evolution spectral width and hence obtain the required digital resolution for J measurement with a smaller number of t_1 increments and/or a smaller *J*-scaling factor. The EXSIDE spectrum of *d*(TTGG) in Fig. 6B was run with the first carbon $\pi/2$ pulse being a band-selective Q5 pulse (*39*) to select only the aromatic carbons.

EXPERIMENTAL

All spectra were recorded at 25°C on a Varian Unity*plus* 500 MHz NMR spectrometer equipped with a programmable pulse modulator in the proton channel, a gradient accessory, and a $^1H\{^{13}C, ^{15}N\}$ triple-resonance probe. All nonselective proton and carbon 90° pulses were of 6.1 and 12.0 μs duration, respectively. All proton band-selective π pulses were Gaussian cascade Q3 pulses (*39*) with phase modulation to achieve off-resonance (single or multiple frequency) inversion. They were generated using the Pandora's Box pulse-shaping program available in Varian NMR software. The strengths of the G_1 and G_2 gradients during the DPFGSE train were 8 and 5 G/cm, respectively, and their duration was 250 and 500 μs, respectively. The encoding gradient (G_3) was of 10 G/cm strength and 1 ms duration while the

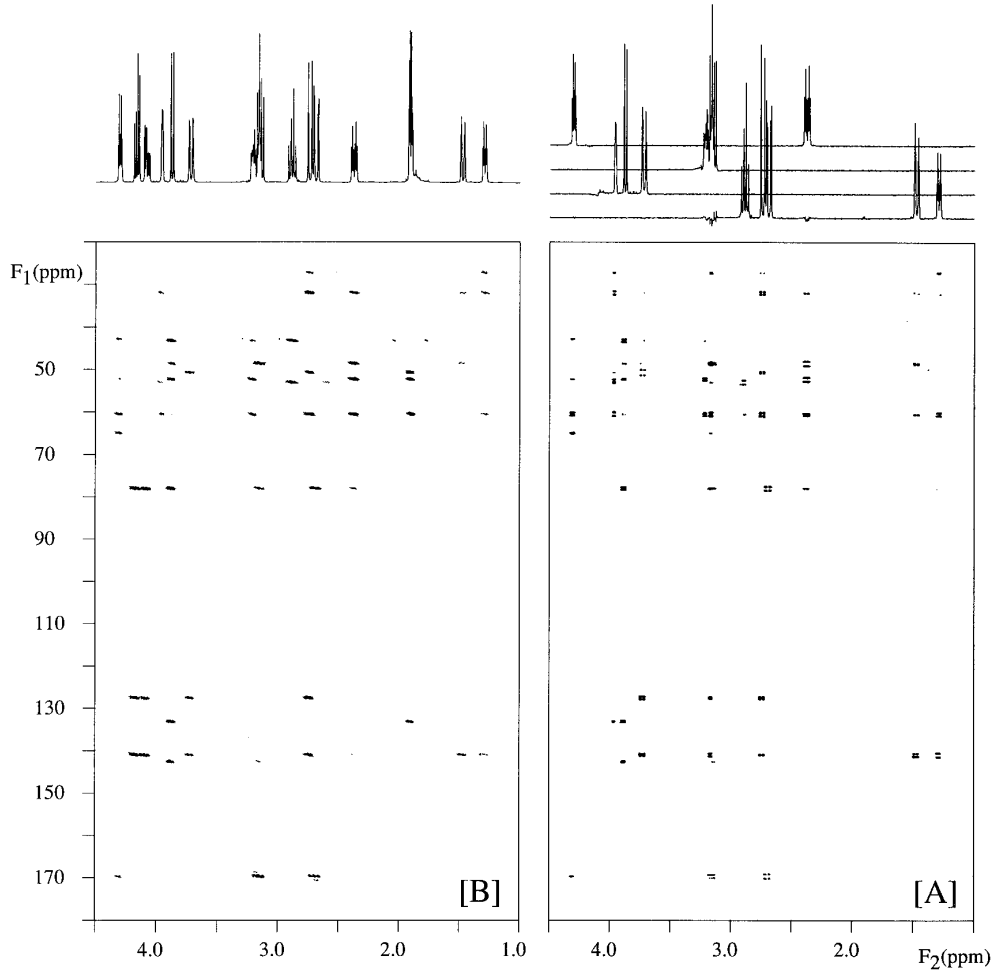

FIG. 4. Comparison of [A] the EXSIDE spectrum with [B] the gradient-selected HMBC spectrum of strychnine in $CDCl_3$ (only the aliphatic ^1H region shown). The EXSIDE spectrum is a superposition of four spectra collected using the four band selections shown. The lengths of the phase-modulated Q3 pulses are as in Fig. 2. All spectra were optimized for 8 Hz coupling (Δ = 63 ms).

decoding gradient (G_4) was of 5 G/cm strength and 500 μs duration. All EXSIDE spectra were recorded as pairs of data with the sign of the decoding gradient (G_4) inverted with respect to each other. The pure P and pure N spectra were then combined during processing to generate pure absorption lineshape. The homospoil gradient (G) strength was typically 10 G/cm and applied for a period of 5 ms. A 100 μs delay followed all gradients for eddy-current recovery. Carbon BB decoupling during acquisition was achieved using GARP1 decoupling modulation. Data were processed using standard Varian software. All EXSIDE spectra were transformed after multiplying the time-domain data with an unshifted Gaussian window function along both the F_1 and F_2 dimensions. The HMBC spectrum in Fig. 4 was transformed after multiplying the time-domain data with an unshifted sine-squared window function along both the F_1 and F_2 dimensions. One-dimensional spectra were transformed without any sensitivity or resolution enhancement.

Spectra for measuring the long-range CH coupling constant, shown in Fig. 3, were run using a sample of 5 mg/ml solution of phenylalanine, with 99% ^{13}C enrichment at the β position, in 50 m*M* NaOD/D_2O. Each EXSIDE spectrum was collected with ^1H and ^{13}C spectral widths of 2000 and 500 Hz centered at 4.8 and 40.5 ppm, respectively. The band-selective Q3 proton π pulses were of 35 ms duration with phase modulation (*35*) to shift its inversion center to -645 Hz, which is the position of the H_α resonance. Two scans of 512 complex points were collected for each of the 64 t_1 increments. The spectra were transformed after zero-filling to 1024×1024 complex points and after linear prediction to 128 complex points along the t_1 dimension.

Band-selective 1D spectra in Fig. 2 and EXSIDE spectra in Figs. 4 and 5 of strychnine were run using a sample of 10 mg/ml solution in $CDCl_3$. The lengths of the band-selective, phase-modulated Q3 pulses used to generate these spectra are given in the respective figures. Each EXSIDE spectrum was collected

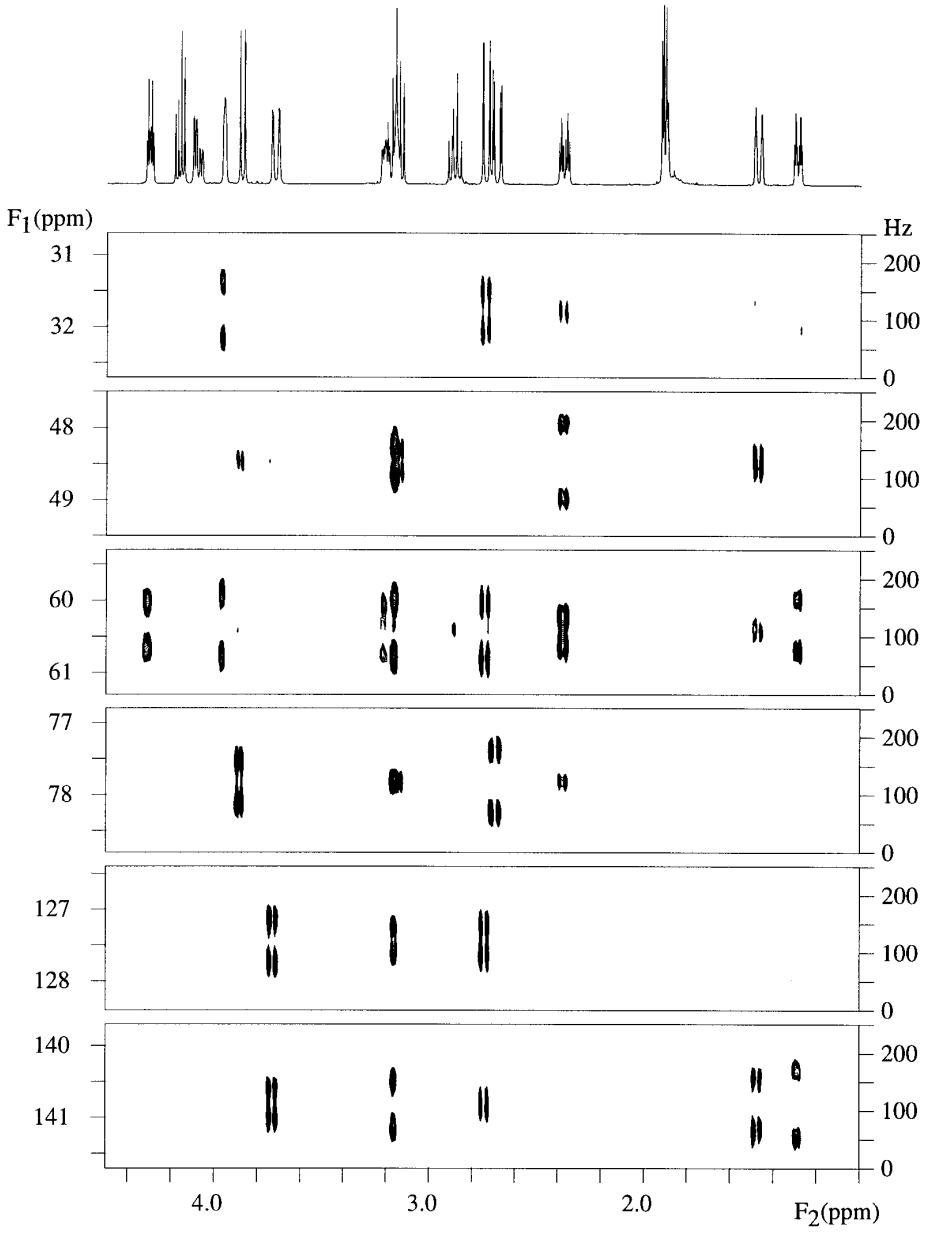

FIG. 5. Selected expansions from the EXSIDE spectrum of strychnine shown in Fig. 4A. Frequency of separation of >40 Hz are resolved and the *J*-scaling factor is 15. This represents a resolvable ''actual'' coupling of approximately 2.7 hertz.

with ^{1}H and ^{13}C spectral widths of 5000 and 22,000 Hz centered at 5.0 and 99 ppm, respectively. Two scans of 2048 complex points were collected for each of the 550 t_1 increments. A *J*-scaling factor (N) of 15 was used. A recovery delay of 1 s was used prior to each scan and the total acquisition time for each of the EXSIDE spectra was 1 h. The spectra were transformed after zero-filling to 2048 × 4096 complex points and after linear prediction to 1100 complex points along the t_1 dimension. The HMBC spectrum of strychnine was collected under the same conditions as the EXSIDE spectra, except that 1100 t_1 increments were collected and the data were processed without any linear prediction.

The EXSIDE spectrum of stachyose (Fig. 6A) was collected using a 5 mM solution in D_2O. Proton and carbon spectral widths were 1000 and 6250 Hz centered at 4.8 and 85 ppm, respectively. The band-selective Q3 proton π pulses were of 10 ms duration with phase modulation (*35*) to shift the inversion center to +200 Hz, which is the center of the anomeric proton resonances. Forty-eight scans of 1024 complex points were collected for each of the 250 t_1 increments. A *J*-scaling factor (N) of 10 was used. A recovery delay of 1.2 s was used prior to each scan and total acquisition time was 15 h. The spectrum was transformed after zero filling to 2048 × 2048 complex points and after linear prediction to 500 complex points along the t_1 dimension.

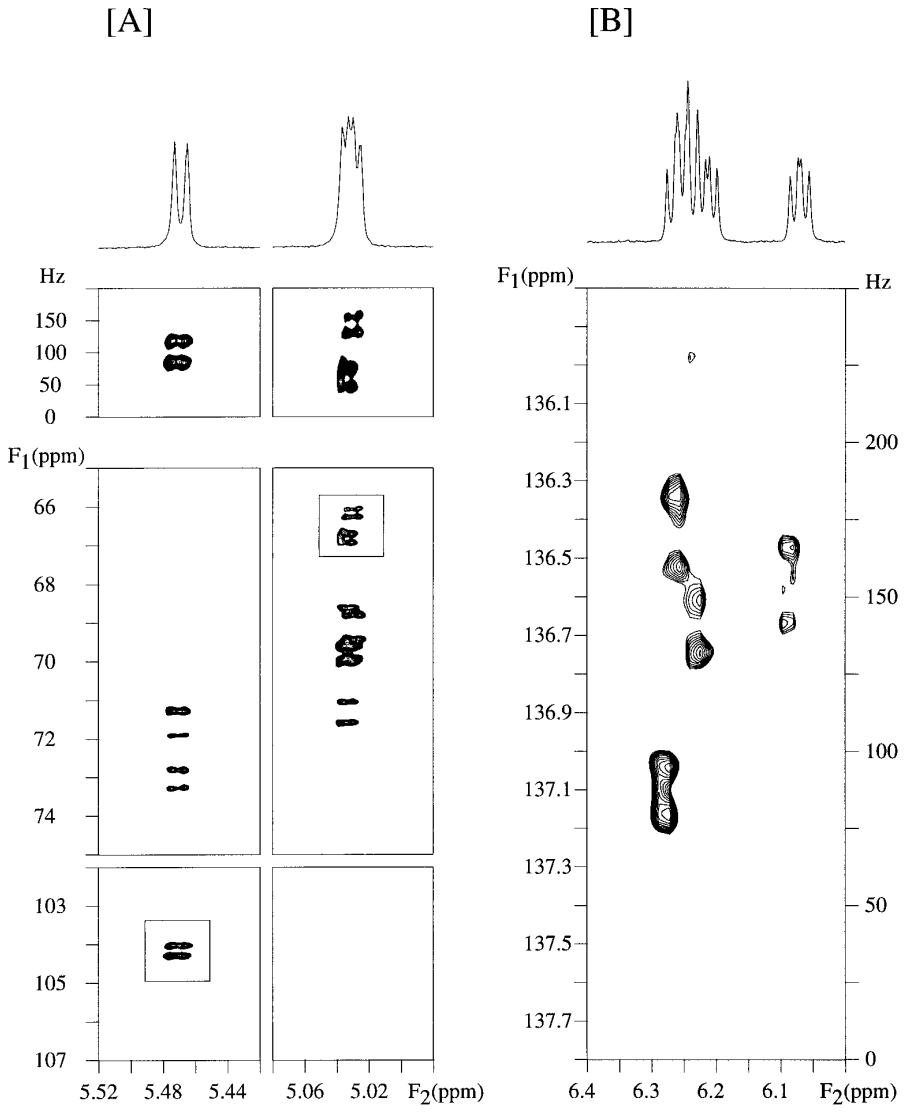

FIG. 6. The EXSIDE spectra of [A] stachyose and [B] *d*(TTGG) in D_2O. Expansion of interresidue cross peaks across the glycosidic linkage is given for stachyose. The spectrum of *d*(TTGG) shown is the H1′–C6/C8 region. Both spectra were recorded with the Δ delay optimized for 5 Hz (=100 ms).

The EXSIDE spectrum of *d*(TTGG) (Fig. 6B) was collected using a 10 m*M* solution (as sodium salt) in D_2O. Proton and carbon spectral widths were 2000 and 1500 Hz centered at 4.8 and 137 ppm, respectively. The band-selective Q3 proton π pulses were of 11.7 ms duration with phase modulation (*35*) to shift the inversion center to +680 Hz, which is the center of the H1′ resonances. The first $\pi/2$ carbon pulse is a band-selective Q5 pulse of 4 ms duration. Eighty scans of 1024 complex points were collected for each of the 150 t_1 increments. A *J*-scaling factor (*N*) of 5 was used. A recovery delay of 1 s was used prior to each scan and total acquisition time was 16 h. The spectrum was transformed after zero-filling to 1024×4096 complex points and after linear prediction to 400 complex points along the t_1 dimension.

SUMMARY

In summary, the *ex*citation-*s*culptured *i*ndirect-*d*etection *e*xperiment (EXSIDE) proposed in this article is a very useful method for measuring long-range heteronuclear coupling constants. The method incorporates two recent advances in NMR techniques, double PFG spin echo (DPFGSE) for band-selective excitation and gradient selection of the coherence-selection pathway. The sequence provides sensitivity comparable to a nonselective gradient HMBC experiment, but with pure absorptive lineshapes. The experiment does not involve any extensive phase cycling and can be run with as little as two scans per t_1 increment. Long-range heteronuclear coupling constants are *J*-scaled and measured along the F_1 (carbon) dimension. Unlike methods where the het-

eronuclear couplings are extracted along the F_2 (proton) dimension with overlapping homonuclear couplings, in the EXSIDE spectrum, the active coupling constant is measured with no interference from any passive couplings. The only prerequisite for the applicability of the EXSIDE sequence is that the resonances of interest be well resolved from any homonuclear-coupled spin partner. As long as one can group a subset of resonances that are not coupled to each other, the method can be used with multifrequency selection. The unique chemical-shift region of anomeric protons in oligosaccharides and the H1′ protons in oligonucleotides makes this method easily applicable for measuring long-range CH coupling constants across the glycosidic bond. In small peptides where the NH and H_α regions are well resolved, this method can be used to measure heteronuclear coupling constants and analyze their relationship to ϕ and ψ angles along the peptide backbone. However, its applicability is expected to be limited in relatively larger molecules due to substantial proton spectral overlap and shorter relaxation rates.

ACKNOWLEDGMENT

The author gratefully acknowledges Dr. Gong-Xin He (Gilead Sciences) for the *d*(TTGG) sample.

REFERENCES

1. G. Wagner, *Methods Enzymol.* 176, 93 (1989).
2. A. Bax, *Methods Enzymol.* 176, 134 (1989).
3. S. W. Fesik and E. R. P. Zuiderweg, *Q. Rev. Biophys.* 23, 97 (1990).
4. L. Müller, *J. Am. Chem. Soc.* 101, 760 (1979).
5. G. Bodenhausen and D. J. Ruben, *Chem. Phys. Lett.* 69, 185 (1980).
6. M. R. Bendall, D. T. Pegg, and D. M. Doddrell, *J. Magn. Reson.* 52, 81 (1983).
7. A. Bax, R. H. Griffey, and B. L. Hawkins, *J. Magn. Reson.* 55, 301 (1983).
8. A. G. Redfield, *Chem. Phys. Lett.* 96, 537 (1983).
9. E. R. P. Zuiderweg, *J. Magn. Reson.* 86, 346 (1990).
10. K. Wüthrich, ''NMR of Proteins and Nucleic Acids,'' Wiley, New York, 1986.
11. M. Karplus, *J. Am. Chem. Soc.* 85, 2870 (1963).
12. G. T. Montelione, M. E. Winkler, P. Rauenbuenhler, and G. Wagner, *J. Magn. Reson.* 82, 198 (1989).
13. G. Wider, D. Neri, G. Ottig, and K. Wuthrich, *J. Magn. Reson.* 85, 426 (1989).
14. A. S. Ediso, W. M. Westler, and J. L. Markley, *J. Magn. Reson.* 92, 434 (1991).
15. M. Kurz, P. Schmieder, and H. Kessler, *Angew. Chem.* 103, 1341 (1991).
16. P. Schmieder, M. Kurz, and H. Kessler, *J. Biomol. NMR* 1, 403 (1991).
17. U. Wollborn and D. Leibfritz, *J. Magn. Reson.* 98, 142 (1992).
18. U. Wollborn, W. Willker, and D. Leibfritz, *J. Magn. Reson. A* 103, 86 (1993).
19. W. Willker, U. Wollborn, and D. Leibfritz, *J. Magn. Reson. B* 101, 83 (1993).
20. J. Keeler, D. Neuhaus, and J. J. Titman, *Chem. Phys. Lett.* 146, 545 (1988).
21. W. Bermel, K. Wagner, and C. Griesinger, *J. Magn. Reson.* 83, 223 (1989).
22. D. G. Davis, *J. Magn. Reson.* 83, 212 (1989).
23. J. J. Titman, D. Neuhaus, and J. Keeler, *J. Magn. Reson.* 85, 111 (1989).
24. L. Poppe and H. van Halbeek, *J. Magn. Reson.* 92, 636 (1991).
25. L. Poppe and H. van Halbeek, *J. Magn. Reson.* 93, 214 (1991).
26. D. Uhrin, A. Mele, K. E. Kover, J. Boyd, and R. A. Dwek, *J. Magn. Reson. A* 108, 160 (1994).
27. W. Willker and D. Leibfritz, *Magn. Reson. Chem.* 33, 632 (1995).
28. M. Eberstadt, G. Gemmecker, D. F. Mierke, and H. Kessler, *Angew. Chem. Int. Ed. Engl.* 34, 1671 (1995).
29. W. Willker, D. Leibfritz, R. Kerssebaum, and W. Bermel, *Magn. Reson. Chem.* 31, 287 (1993).
30. P. L. Rinaldi and P. A. Keifer, *J. Magn. Reson. A* 108, 259 (1994).
31. A. L. Davis, J. Keeler, E. D. Laue, and D. Moskau, *J. Magn. Reson.* 98, 207 (1992).
32. J. Boyd, N. Soffe, B. K. John, D. Plant, and R. Hurd, *J. Magn. Reson.* 98, 660 (1992).
33. K. Scott, J. Stonehouse, J. Keeler, T. L. Hwang, and A. J. Shaka, *J. Am. Chem. Soc.* 117, 4199 (1995).
34. G. A. Morris, *J. Am. Chem. Soc.* 102, 428 (1980).
35. S. L. Patt, *J. Magn. Reson.* 96, 94 (1992).
36. G. Bodenhausen and R. R. Ernst, *J. Am. Chem. Soc.* 104, 1304 (1982).
37. A. Bax and S. S. Pochapsky, *J. Magn. Reson.* 99, 638 (1992).
38. S. Wimperis and R. Freeman, *J. Magn. Reson.* 58, 348 (1984).
39. L. Emsley and G. Bodenhausen, *J. Magn. Reson.* 97, 135 (1992).
40. E. Kupce and R. Freeman, *J. Magn. Reson. A* 105, 234 (1993).